RESEARCH ARTICLE

ELECTROPHORESIS

Rapid prototyping of polydimethylsiloxane (PDMS) microchips using electrohydrodynamic jet printing: Application to electrokinetic assays

Anupam Choubey | **Kaushlendra Dubey** | **Supreet Singh Bahga** [ORCID]

Department of Mechanical Engineering, Indian Institute of Technology Delhi, New Delhi, India

Correspondence
Supreet Singh Bahga, Department of Mechanical Engineering, Indian Institute of Technology Delhi, 110016, New Delhi.
Email: bahga@mech.iitd.ac.in

Color online: See article online to view Figures 1–3 in color.

Abstract

Polydimethylsiloxane (PDMS) based microfluidic devices have found increasing utility for electrophoretic and electrokinetic assays because of their ease of fabrication using replica molding. However, the fabrication of high-resolution molds for replica molding still requires the resource-intensive and time-consuming photolithography process, which precludes quick design iterations and device optimization. We here demonstrate a low-cost, rapid microfabrication process, based on electrohydrodynamic jet printing (EJP), for fabricating non-sacrificial master molds for replica molding of PDMS microfluidic devices. The method is based on the precise deposition of an electrically stretched polymeric solution of polycaprolactone in acetic acid on a silicon wafer placed on a computer-controlled motion stage. This process offers the high-resolution (order 10 µm) capability of photolithography and rapid prototyping capability of inkjet printing to print high-resolution templates for elastomeric microfluidic devices within a few minutes. Through proper selection of the operating parameters such as solution flow rate, applied electric field, and stage speed, we demonstrate microfabrication of intricate master molds and corresponding PDMS microfluidic devices for electrokinetic applications. We demonstrate the utility of the fabricated PDMS microchips for nonlinear electrokinetic processes such as electrokinetic instability and controlled sample splitting in ITP. The ability to rapid prototype customized reusable master molds with order 10 µm resolution within a few minutes can help in designing and optimizing microfluidic devices for various electrokinetic applications.

KEYWORDS
electrokinetics, electrohydrodynamic jet printing, microchip electrophoresis, soft lithography

1 | INTRODUCTION

The advancements in microfabrication have led to the development of miniaturized lab-on-a-chip systems for integrating and performing various biochemical analyses techniques. The efforts to develop lab-on-a-chip systems

---

were originally driven by the interest in miniaturizing electrophoretic and electrokinetic systems for enhanced performance and reduced analysis time [1, 2]. The integration of various electrophoresis techniques, including capillary zone electrophoresis (CZE) and isotachophoresis (ITP) on a microchip format, have been major commercial successes of microfluidic technology [3, 4].

Microfluidic devices for electrophoretic and electrokinetic assays are typically fabricated using wet etching of glass, which is not amenable to rapid prototyping and customization. Moreover, the necessity of a clean room facility, cumbersome glass bonding method, and the need for skilled personnel for fabricating glass microfluidic devices result in the high cost of the devices [5]. To overcome the challenges in fabricating glass microfluidic devices, alternative methods based on elastomers such as polydimethylsiloxane (PDMS) and thermoplastic polymers such as polymethylmethacrylate (PMMA) have been developed [5–8]. Over the years, PDMS has become the material of choice for fabricating cost-effective microfluidic devices as it offers favourable optical properties like glass, is biodegradable, and is thermally and electrically insulating [9]. PDMS-based microfluidic devices with feature sizes of the order of 10 μm can be easily fabricated using the replica molding process, wherein PDMS is poured on the master mold and cured to get a negative replica of the master. Thereafter, the negative replica is bonded to another PDMS or a glass substrate to form a tight seal [7]. While replica molding of PDMS devices allows inexpensive replication of microfluidic devices from the master mold in a laboratory setting, the method also lacks the capacity for rapid customization. This limitation is due to the need for microfabrication of master molds with expensive photolithography or electron beam lithography process, which requires skilled personnel and a clean room facility [10]. Consequently, master mold fabrication is typically outsourced to central facilities, which precludes rapid design iterations and device customization.

Various alternatives to photolithography have been explored to fabricate customized master molds for replica molding. These include mold fabrication using 3D printing [11, 12], laser ablation [13], micro-milling [14], and xurography [15]. The primary limitation of the above-mentioned alternative methods is that the morphology of the mold features depends on the dimension of the nozzle or the machining tool for additive and subtractive manufacturing processes, respectively. Consequently, the minimum feature size obtained using these methods is of order 100 μm in contrast to 10 μm or smaller feature sizes obtained using photolithography. Moreover, mold fabrication using the subtractive-manufacturing processes often involves an additional step of preparing a male mold

from a female mold [13, 14], making the process tedious and material-consuming.

Typical microfluidic applications, including electrokinetic assays, require microchannel width and depth of order 10 μm as small device dimensions provide better heat dissipation and low sample dispersion [16]. Therefore, there is a need for a micromanufacturing technique for which the feature morphology does not depend on the tool size, offers high resolution, is flexible in constructing complex features, and favours customization. Recently, electrohydrodynamic jet printing (EJP) has emerged as a promising direct ink writing (DIW) method for high-resolution printing of customized polymeric structures with micrometer resolution. In EJP, a polymeric solution or melt is flown through a needle onto a motion-controlled substrate, and a large potential difference is applied between the nozzle and the substrate. The high electric field ($\sim 10^4$ V/cm) deforms the spherical meniscus of the polymeric ink at the nozzle tip into a cone, called a Taylor cone [17] (see Supporting Information). For a specific range of applied voltage difference and flow rate, a stable jet emerges from the cone tip, whose radius is relatively independent of the nozzle diameter [18]. Consequently, micrometer resolution features can be patterned [18], while using a large-diameter nozzle to prevent clogging. The comparison of EJP with standard microfabrication techniques (presented in Table S1) suggests that EJP is more suitable for rapid prototyping of high-resolution customized master molds.

While the use of EJP has been demonstrated for various applications such as printing polymeric scaffolds, microlens arrays, and footpaths for electronic circuits [18], its capability to print reusable master molds for replica molding of elastomeric microfluidic devices has still not been fully explored. The only reported work in the literature on EJP-based master mold fabrication are those by Coppola et al. [19], and Chi et al. [20], who fabricated sacrificial master molds of poly(D,L-lactide-co-glycolide) (PLGA) and wax for replica molding of microfluidic devices. Unlike the reusable molds obtained from photolithography or electron beam lithography, the molds fabricated by Coppola et al. and Chi et al. can be used only once for fabricating microfluidic devices.

In the current work, we demonstrate a low-cost, additive microfabrication method using EJP to fabricate reusable master molds for replica molding of PDMS microfluidic chips for electrokinetic and electrophoretic assays. To this end, we use a customized polymeric ink to print high-resolution master molds on a silicon wafer substrate with a feature resolution of order 10 μm within a few minutes. In particular, we demonstrate the printing of reusable molds with a straight line, cross-shaped and Y-shaped features. We then demonstrate the use of PDMS

devices replicated from these molds for two electrokinetic applications: (i) electrokinetic instability and (ii) sample preconcentration and controlled splitting of the stacked sample using ITP. The ability to rapid prototype customized reusable master molds with 10 μm resolution within a few minutes can help in the iterative design and optimization of microfluidic devices.

2 | MATERIALS AND METHODS

2.1 | Experimental setup for EJP

Figure 1 schematically shows the various components of an electrohydrodynamic jet (EHD-jet) printer consisting of a metallic needle, a collector plate, a high voltage DC power supply unit (Ionics, 0−5 kV, 10 mA), and a polymeric solution feeding system. The collector plate and the needle are mounted on high-precision motorized stages (Newport, model XPS-D, USA), having motions along x-y and z directions, respectively. The substrate was mounted on x-y linear stage having a travel distance of 140 mm and 100 mm with 1 μm incremental motion in each direction. The nozzle was mounted on a linear stage, having a travel distance of 40 mm with 0.1 μm incremental motion to vary the nozzle to substrate distance.

The precision stages were connected to a motion controller (Newport), which in turn was connected to a computer through a serial LAN port. The solution feeding system consists of a standard 2.5 ml syringe having an inner diameter (I.D.) = 8.5 mm and a flexible hose having I.D. = 1.5 mm connecting the syringe and the nozzle. We used nozzles made of stainless-steel of 25G (I.D.

= 0.25 mm, L = 25 mm) and 27G (I.D. = 0.21 mm, L = 25 mm) grades. The polymeric solution was pumped using a computer-controlled syringe pump (Cole-Parmer, dispensing accuracy of ±0.3%, repeatability of ±0.05%). The positive terminal of the power supply was connected to the metallic nozzle, whereas the substrate was grounded to complete the electric circuit. The master molds were fabricated by printing polymeric features on a polished p-type silicon wafer (conductivity range = 10−100 S/m) of diameter two-inch and thickness of 0.5 mm.
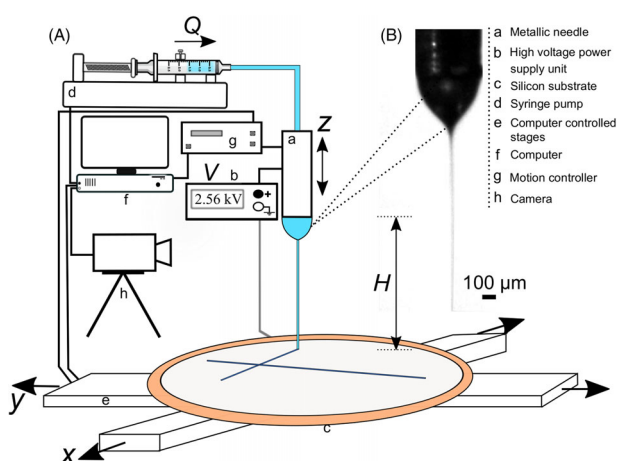
The position, the motion of the stages, the flow rate of the polymeric solution, and the potential difference across the needle and the substrate were controlled using an in-house developed programmable LABVIEW virtual interface. The printing process was monitored by a CMOS camera (IDS, UI-1220LE-M-HQ, 6 μm pixel size) fitted with the zoom lens.

2.2 | Solution preparation

Among various polymeric solutes commonly used for EJP such as PEO (polyethylene oxide), PCL (polycaprolactone), PVP (polyvinylpyrrolidone), and PLGA, we used PCL (polycaprolactone, average $M_n \sim$ 45,000 Da, Sigma Aldrich) as it is a non-toxic, biocompatible and biodegradable polymer with good mechanical properties [21]. In the solvent-based EJP process, an essential requirement for adequate printing is the quick solidification of the polymeric ink during deposition on the substrate. To this end, a high polymeric concentration must be used for printing to ensure rapid solidification of the polymeric fibers over a short distance between the needle and the collector plate (stand-off distance). Therefore, we prepared a polymeric solution with a concentration of 40% (w/v) for the experiments reported here by dissolving PCL in acetic acid (CH_3COOH, Sigma–Aldrich, 99.7% pure). To obtain a homogeneous solution, we gradually dissolved the PCL pellets in acetic acid and simultaneously stirred the combination using a magnetic stirrer at 700 rpm and 40°C for a period of 7−12 hrs. We finally degassed the polymeric ink for 20−30 mins to remove any notable air bubbles. To avoid solidification, the polymeric ink was stored at 30°C. Following a similar procedure, we also successfully prepared and tested PCL in acetic acid solutions with concentrations ranging from 30% to 60% suitable for EJP.

FIGURE 1 Schematic showing the experimental setup used for EHD-jet printing of master molds. (A) The setup consists of a metallic needle, collector plate, liquid dispensing system and high voltage DC source. (B) A representative snapshot of a stable cone-jet during the experiments performed using 40% (w/v) PCL solution.
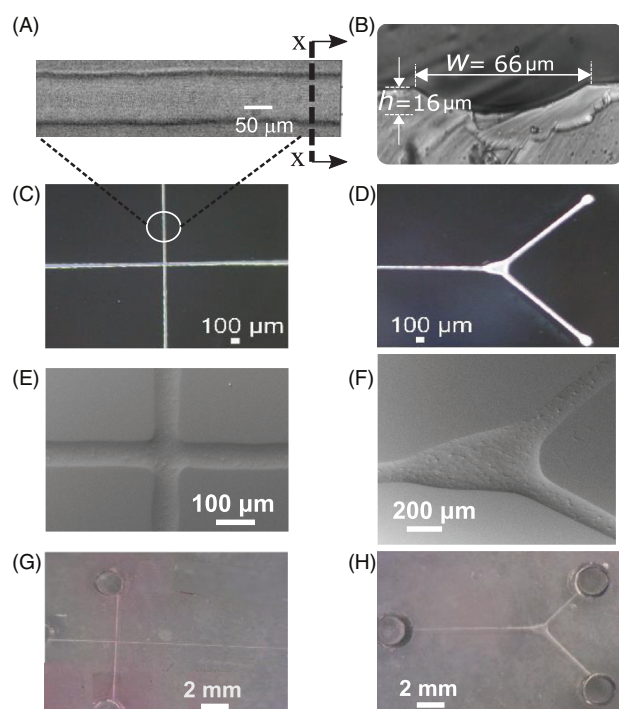
2.3 | Master mold and microchip fabrication

Following the procedure mentioned above, we printed straight line, cross and Y-shaped features on a silicon

substrate using the 25G nozzle and 40% (w/v) PCL in acetic acid solution. For all these experiments, we maintained a small stand-off distance of $H = 4$ mm between the needle and the collector to suppress the whipping instability observed in the electrospinning process. We maintained a high stage speed of $V_{stage} = 50$ mm/s to achieve stable printing of fine features. The detailed effect of the process parameters on the printed features is described in the Supporting Information. The printing of a typical structure, such as a cross-shaped feature, takes a minute. We used the substrates with printed features as the master molds for developing the corresponding microfluidic devices through the standard replica molding process (see protocol in Supporting Information). Further, to confirm the non-sacrificial nature of the master mold, we performed replica molding several times on the master mold and found that the printed features remained intact even after twelve repetitions. Finally, the negative replica of the master mold in PDMS was bonded to a glass slide after plasma treatment (Harrick Plasma, PDC-32G-2) for 50 s at 212 mtorr vacuum pressure to obtain the final microfluidic device. Figure 2A–H shows the master molds, PDMS replica, and

plasma-bonded PDMS devices. First, we printed a straight line feature to check the morphology, resolution, and continuity of the deposited ink on the substrate. For printing the straight line feature, the solution was fed at a rate of 0.2 µl/min and the applied potential was set at 2.56 kV. Figure 2A shows the PDMS microchannel replicated from the printed straight line. We measured the width (w) and depth (h) of the obtained microchannel by observing a cut section of the channel under an optical microscope (Nikon Eclipse, TS100, Japan) with 20× objective lens (CFI Achromat, LWD, NA = 0.40). The measured lateral dimensions were $w = 66$ µm and $h = 16$ µm, as shown in Figure 2B. Thereafter, we printed the cross-shaped and T-shaped features of the same dimensions using the same experimental conditions, as shown in Figure 2C and Figure S4B, respectively. The length of each channel segment connecting the north (N), west (W), and south (S) reservoirs to the junction was 5 mm, whereas the length of the channel segment from the junction to the east (E) reservoir was 15 mm. The edges of the replicated straight line, and cross-shaped microchannels show a high degree of straightness, as shown in Figures 2A and 2E. The top view of the cross-shaped PDMS microfluidic device is shown in Figure 2G.

Next, we printed a Y-shaped geometry using different operating conditions. Figures 2D and 2F show the printed master mold and the corresponding PDMS-based negative replica of the Y-shaped feature. We printed the feature at the applied voltage $V = 2.45$ kV while the flow rate was maintained at $Q = 0.52$ µl/min.

For the Y-shaped microchannel, the top view is shown in Figure 2H, the length of the channel segment from the west end to the junction was 15 mm, and each branch from the junction was 5 mm long. The width, height, and length of the microchannels are provided in Table 1. Besides these devices, we fabricated high-resolution master molds for various other designs such as mesh, gradient generator, and cross with a bifurcation, details of which have been provided in the supporting information.

Here, we also note that the microchannels obtained from the EHD-jet printed master molds are of circular cross-section, similar to other inkjet printing processes, as shown in Figure 2B. The circular cross-sectional shape of the microchannel is a characteristic of this fabrication process, just as wet etching, laser ablation and

FIGURE 2 Microfabricated master molds, PDMS replicas, and PDMS microchips. (A) Negative replica of the printed straight line feature and (B) cross-section of the microchannel. Panels (C) and (D) show the master molds with cross-shaped and Y-shaped features, respectively. Panels (E) and (F) show the SEM images of negative PDMS replicas obtained from the corresponding master molds. Panels (G) and (H) show the top views of the final microfluidic devices obtained after plasma bonding with glass slides.

TABLE 1 Dimensions of fabricated microfluidic channels.

SI No.	Channel feature	Width (µm)	Height (µm)	Length of channel (mm)
1	Straight line	66, 80, 120	16, 20, 25	30
2	Cross-shaped	66	16	20
3	Y-shaped	120	25	20

photolithography are characterised by D-shaped, Gaussian-shaped and rectangular cross-sections, respectively [22].

2.3.1 | Accuracy of the master molds and negative replicas

In this section, we discuss in detail about the replication fidelity, repeatability and uniformity of the printed features. At the outset, we measured the width of the printed features and the corresponding PDMS-based replicas after the twelfth iteration of replica molding. For cross-shaped geometry, the mean width of the printed feature and the corresponding negative replica was measured as 66.5±1.5 μm and 66.0±1.5 μm, respectively. Similarly for Y-shaped geometry, the mean width of the mold and replica was 120.7±1.4 μm and 120.0±1.4 μm, respectively. Figure S6 compares the widths of the master molds and negative replicas corresponding to cross and Y-shaped features. In both cases, at a 95% confidence level, the difference in the mean line widths for mold and replica is smaller than the uncertainty in the widths. This suggests that the mold dimensions do not alter during the replication process, confirming the non-sacrificial nature of the master molds with good replication fidelity.

Similarly, to check the repeatability of the printing process, we printed ten straight lines using the 25G nozzle at two different time instances with the same ambient conditions. The operating conditions were kept fixed at $Q = 0.2$ μl/min, $V = 2.56$ kV, $V_{stage} = 50$ mm/s, and $H = 4$ mm in both experiments. The difference in the mean widths of the lines printed at two different time instances was 0.3 ± 1.7 μm at a confidence level of 95%. So, we can not statistically conclude that the mean widths corresponding to both sets of experiments are different; hence, the experiments can be considered repeatable.

Next, to check the uniformity of the printed line, we measured the line width at ten different locations along the axial direction. We repeated this process for each of the ten straight lines printed at $Q = 0.2$ μl/min, $V = 2.56$ kV, $V_{stage} = 50$ mm/s and $H = 4$ mm. The axial variability in the line width estimated using $t-$distribution for each of the ten lines was $< 2\%$, which advocates the uniformity of the printed features. However, we would like to highlight three important factors that cause non-uniformities in the printed features. Firstly, the accumulation of an additional volume of ink at the cross-over and the junction points leads to the spreading of the ink resulting in a localized non-uniformity. Consequently, the dimensions at the cross-over point (as in the cross-shaped feature) and at the junction point (as in the Y-shaped feature) are higher than

the remaining parts of the respective features, as shown in Figure 2C–F, respectively. Also, the spreading around the junction point is more in the Y-shaped feature than that in the cross-shaped feature, as can be seen in Figures 2E and 2F. This is because the horizontal segment of the cross-feature got sufficient time to solidify before the vertical line was printed over it. On the other hand, for the Y feature, the printed segment near the junction got insufficient time to solidify before the two branches were printed via the junction point, resulting in higher width near the junction. The geometrical non-uniformity due to overlapping structures is an artefact of continuous EJP and can be minimized but not fully avoided by choosing a suitable stand-off distance, ensuring adequate solidification of the fiber during its travel from the needle tip to the substrate.

Secondly, the residual charges on the substrate may affect the stability and uniformity of the printed features. The charge relaxation time of the substrate ($\tau_c = \varepsilon/K \sim 10^{-12}-10^{-11}$ s for p-type Si wafer) and the lifetime of the jet ($t_{jet} = \pi d_{jet}^2 H/Q \sim 10^{-4}-10^{-3}$ s) are the two characteristic time scales that determine whether uniform features can be deposited on the substrate or not. For $\tau_c \ll t_{jet}$ as in the case of conductive and semiconductive substrates, uniform features can be deposited on the substrate [23]. In our case, non-uniformity due to charge accumulation did not occur as we used a sufficiently conductive p-type silicon wafer.

Lastly, the small undulations observed along the edges of the mold are mainly due to the inhomogeneous solvent evaporation from the printed feature causing aggregation of the polymer near the edges. This ultimately leads to convective capillary flow from regions of high polymer concentration to low polymer concentration, causing undulations along the edges [24]. Despite the presence of these undulations, the axial variability in width for the cross and the Y-shaped features are well within 3% and 2% of their respective mean widths.

3 | APPLICATIONS OF FABRICATED DEVICES

In this section, we demonstrate the use of our in-house fabricated PDMS microfluidic devices for two non-linear electrokinetic processes. The cross-shaped microchip was used to perform electrokinetic instability (EKI) experiments, whereas the Y-shaped microchip was used to perform sample preconcentration using ITP, followed by sample splitting at the Y junction. Note that, we used PDMS devices a week after plasma bonding and after such a time gap the PDMS surface attains its intrinsic surface zeta potential [25]. For both of these experiments, the electrolyte solutions were prepared by diluting respective

1 M stock solutions with de-ionized water. An inverted epifluorescence microscope (Nikon Eclipse, TS100, Japan) equipped with a collimated LED light source (Thorlabs, USA) and Nikon G2-A filter set (510−560 nm band-pass excitation filter and 590 nm long-pass barrier filter) was used to visualize the fluorescent species. A high voltage DC power supply unit (Ionics, 5 kV, 10 mA) was used to apply high electric potential at the reservoirs using platinum wires as the electrodes. All the experimental observations corresponding to EKI and ITP were recorded using a CCD camera (pco.pixelfly, Germany). The raw images were corrected for background noise and normalized with flat-field images.
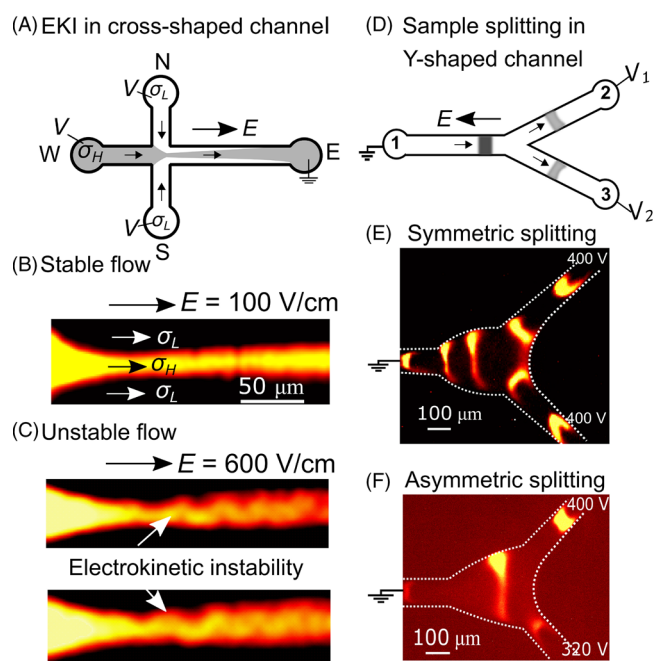
3.1 | Electrokinetic instability

We performed experiments on electrokinetic instability that develops during electroosmotic flow with stream-wise conductivity gradients [26]. In particular, we performed EKI experiments similar to those of Posner et al. [26] and Dubey et al. [27], wherein a high-conductivity fluid flows in between two low-conductivity sheath streams, as illustrated in Figure 3A. The high and low-conductivity electrolyte solutions consisted of 200 mM HEPES and 100

mM NaOH and 200 μM HEPES and 100 μM NaOH, respectively. The measured conductivity ratio (σ_H/σ_L) was 640. We chose a high-conductivity ratio for our experiments so as to observe the instability at a relatively low-electric field.

Figure 3A shows the experimental configuration of EKI experiments in the cross-shaped PDMS device. We filled the W reservoir with the high-conductivity electrolyte solution, while the N and S reservoirs were filled with the low-conductivity electrolyte solution. To visualize the instability, we mixed an electrically neutral fluorescent tracer, rhodamine-B, into the center stream. Application of electric field (E) causes the electrolyte solutions to flow from the N, W, and S reservoirs towards the junction where the low-conductivity streams hydrodynamically squeeze the high-conductivity stream. Thereafter, the high-conductivity stream and two low-conductivity sheath streams convect towards the E reservoir.

Figures 3B and 3C show the experimental results obtained at two different electric field values. At a low electric field, E = 100 V/cm, the flow remains stable as no significant perturbations are observed, as can be seen in instantaneous snapshots in Figure 3B. The high-conductivity stream at the center convects and gradually expands across the channel due to molecular diffusion. At a higher electric field, E = 600 V/cm, unstable fluid motion is observed in the flow. At this condition, a sinusoidal disturbance emerges at the interface between high- and low-conductivity streams, as shown in Figure 3C. The EKI is characterized by these disturbances resulting in the rapid mixing of the fluid streams over a short distance from the junction. The sinusoidal flow structures are qualitatively similar to those observed in similar experiments performed by Posner et al. [26] and Dubey et al. [27]. However, we observed the flow instability at a higher electric field as compared to those by Posner et al. and Dubey et al. This is attributed to the small channel height of our fabricated PDMS device, which has a stabilizing effect on the instability. Moreover, the electroosmotic mobility of the native PDMS surface is lower than that of glass used in previous studies, resulting in a thicker interface between high and low-conductivity streams and, consequently, a higher threshold for the onset of instability.

3.2 | Isotachophoresis

Next, we used the Y-junction device to perform ITP preconcentration of a fluorescent analyte. In ITP, ionic species are focused and preconcentrated between zones of a leading electrolyte (LE) and a trailing electrolyte (TE) under the effect of the applied electric field. Firstly, we performed experiments using the Y-junction device similar to those of Persat et al. [28], wherein preconcentration of fluorescent

FIGURE 3 Experimental demonstration of cross-shaped and Y-shaped PDMS device. (A) Schematic shows the base state of EKI. (B)-(C) Stable and unstable flow. (D) Schematic showing the ITP experiments in the Y-shaped channel. (E) Symmetric splitting and (F) asymmetric splitting of the focused analyte zone due to the application of the same and different potentials at the two ends of the Y channel, respectively.

analyte is done in the anionic ITP followed by controlled sample splitting at the Y-junction, as shown in Figure 3D. To this end, we used 340 mM TRIS (Sigma-Aldrich) and 150 mM HEPES as TE, while 150 mM TRIS and 50 mM HCl (hydrochloric acid, CDH, India) as LE. We added 1% PVP (polyvinylpyrrolidone) in both electrolyte solutions to suppress the electroosmotic flow [29]. The sample analyte, fluorescein, was mixed with the TE for continuous sample preconcentration.

To perform ITP experiments, initially, all the channel segments of the Y microchannel were filled with LE solution from reservoirs 2 and 3 by applying a vacuum at reservoir 1 (Figure 3D). Reservoir 1 is then rinsed with DI water and filled with the TE-sample mixture. High electric potentials V_1 and V_2 were applied at reservoirs 2 and 3 while reservoir 1 was grounded, as shown in Figure 3D As soon as the electric field (E) was applied, fluorescein got stacked between LE and TE zones. The focused analyte zone migrated in the direction opposite to the direction of the applied electric field towards the Y-junction and bifurcated into two distinct zones.

In Figure 3E, we show the peak of stacked fluorescein at various time instances by overlaying the instantaneous snapshots. In the first set of experiments, we applied equal electric potentials $V_1 = V_2 = 400$ V at reservoirs 2 and 3, resulting in symmetric splitting in the upper and lower branches (Figure 3E). As suggested by Persat et al., the splitting of the focused sample can be controlled by varying the electric field in each branch of the Y-channel. To show the asymmetric splitting, we performed another experiment where we applied different potentials $V_1 = 400$ V and $V_2 = 320$ V at reservoirs 2 and 3, respectively. As a result, the fraction of the total sample that bifurcates into the upper branch is more than that in the lower branch, as can be seen in Figure 3F. Besides these experiments, we also performed anionic peak-mode ITP experiments in the cross-shaped microchannel, and the corresponding experimental results are provided in Supporting Information.

4 | CONCLUDING REMARKS

We have demonstrated the use of EHD-jet printing (EJP) for rapid and low-cost fabrication of customizable and non-sacrificial master molds for replica molding of microfluidic devices. We performed several experiments using PCL 40% (w/v) solution to show the effect of operating parameters on the morphology of the printed features. Our study shows that the width of the printed feature scales with flow rate as $w \sim Q^{1/3}$ (see supporting information). Also, an increase in the applied electric field and the stage speed results in a finer feature. After configuring the suitable operating parameters, we printed uniform (uncertainty in width < 3%) and high-resolution ($\sim$10 μm) features on the silicon wafer, which subsequently acts as a master mold for microfluidic device fabrication. In particular, we demonstrated mold and device fabrication of the cross-shaped and the Y-shaped microfluidic devices using the current method to demonstrate two highly nonlinear electrokinetic applications that are routinely used in lab-on-a-chip systems: (i) electrokinetic instability (EKI), and (ii) sample preconcentration and controlled splitting of the stacked sample using ITP. The EKI and ITP experiments in the fabricated microfluidic devices are in good agreement with those in the literature.

The microfabrication method presented here is quick and inexpensive as no photomask is involved in preparing the master molds. Also, the substrate with the printed features is used directly as the mold, which allows rapid customization. Most importantly, the morphology of the printed feature is independent of the needle diameter used for EJP, which allows high-resolution printed features with good replication fidelity. Hence, the ability to print customized designs on a single substrate makes the method highly suitable for iterative design and optimization of microfluidic devices.

CONFLICT OF INTEREST STATEMENT
The authors have declared no conflict of interest.

DATA AVAILABILITY STATEMENT
Data is available within the article and the supplementary materials.

ORCID
Supreet Singh Bahga https://orcid.org/0000-0001-7277-9015

REFERENCES
1. Székely L, Guttman A. New advances in microchip fabrication for electrochromatography. Electrophoresis. 2005;26: 4590–604.
2. Scott SM, Ali Z. Fabrication methods for microfluidic devices: An overview. Micromachines. 2021;12:319.

3. Landers JP. Handbook of capillary and microchip electrophoresis and associated microtechniques. Boca Raton: CRC press; 2007.

4. Bahga SS, Santiago JG. Coupling isotachophoresis and capillary electrophoresis: a review and comparison of methods. Analyst. 2013;138:735–54.

5. Wang J, Pumera M, Chatrathi MP, Escarpa A, Konrad R, Griebel A, et al. Towards disposable lab-on-a-chip: Poly(methylmethacrylate) microchip electrophoresis device with electrochemical detection. Electrophoresis. 2002;23:596–601.

6. Sia SK, Whitesides GM. Microfluidic devices fabricated in poly(dimethylsiloxane) for biological studies. Electrophoresis. 2003;24:3563–76.

7. McDonald JC, Duffy DC, Anderson JR, Chiu DT, Wu H, Schueller OJ, et al. Fabrication of microfluidic systems in poly (dimethylsiloxane). Electrophoresis. 2000;21:27–40.

8. Horng RH, Han P, Chen HY, Lin KW, Tsai TM, Zen JM. PMMA-based capillary electrophoresis electrochemical detection microchip fabrication. J Micromech Microeng. 2004;15:6–10.

9. Tang SKY, Whitesides GM. Basic microfluidic and soft lithographic techniques. Fainman Y, Lee LP, Psaltis D, Yang C, editors. New York: McGraw-Hill; 2010.

10. Thompson LF. An introduction to lithography. ACS Publications; 1983.

11. Hwang Y, Paydar OH, Candler RN. 3D printed molds for non-planar PDMS microfluidic channels. Sens Actuators A. 2015;226:137–42.

12. Ching T, Li Y, Karyappa R, Ohno A, Toh YC, Hashimoto M. Fabrication of integrated microfluidic devices by direct ink writing (DIW) 3D printing. Sens Actuators B. 2019;297:126609.

13. Isiksacan Z, Guler MT, Aydogdu B, Bilican I, Elbuken C. Rapid fabrication of microfluidic PDMS devices from reusable PDMS molds using laser ablation. J Micromech Microeng. 2016;26:035008.

14. Wilson ME, Kota N, Kim Y, Wang Y, Stolz DB, LeDuc PR, et al. Fabrication of circular microfluidic channels by combining mechanical micromilling and soft lithography. Lab Chip. 2011;11:1550–5.

15. Speller NC, Morbioli GG, Cato ME, Cantrell TP, Leydon EM, Schmidt BE, et al. Cutting edge microfluidics: Xurography and a microwave. Sens Actuators B. 2019;291:250–6.

16. Ramachandran A, Santiago JG. Isotachophoresis: Theory and microfluidic applications. Chem Rev. 2022;122:12904–76.

17. Taylor GI. Disintegration of water drops in an electric field. Proc Math Phys Eng Sci. 1964;280:383–97.

18. Onses MS, Sutanto E, Ferreira PM, Alleyne AG, Rogers JA. Mechanisms, capabilities, and applications of high-resolution electrohydrodynamic jet printing. Small. 2015;11:4237–66.

19. Coppola S, Nasti G, Todino M, Olivieri F, Vespini V, Ferraro P. Direct writing of microfluidic footpaths by pyro-EHD printing. ACS Appl Mater Interfaces. 2017;9:16488–94.

20. Chi X, Zhang X, Li Z, Yuan Z, Zhu L, Zhang F, et al. Fabrication of microfluidic chips based on an EHD-assisted direct printing method. Sensors. 2020;20:1559.

21. Cai S, Sun Y, Wang Z, Yang W, Li X, Yu H. Mechanisms, influencing factors, and applications of electrohydrodynamic jet printing. Nanotechnol Rev. 2021;10:1046–78.

22. Lee SJJ, Sundararajan N. Microfabrication for microfluidics. Norwood, Ma: Artech House. 2010.

23. Bu NB, Huang YA, Yin ZP. The effect of substrate on continuous electrohydrodynamic printing: Adv Mater Res. 2013;684:352–356.

24. Mkhize N, Bhaskaran H. Electrohydrodynamic jet printing: Introductory concepts and considerations. Small Science. 2022;2:2100073.

25. Saucedo-Espinosa MA, Lapizco-Encinas BH. Refinement of current monitoring methodology for electroosmotic flow assessment under low ionic strength conditions. Biomicrofluidics. 2016;10:033104.

26. Posner JD, Santiago JG. Convective instability of electrokinetic flows in a cross-shaped microchannel. J Fluid Mech. 2006;555:1–42.

27. Dubey K, Gupta A, Bahga SS. Coherent structures in electrokinetic instability with orthogonal conductivity gradient and electric field. Phys Fluids. 2017;29:092007.

28. Persat A, Santiago JG. Electrokinetic control of sample splitting at a channel bifurcation using isotachophoresis. New J Phys. 2009;11:075026.

29. Milanova D, Chambers RD, Bahga SS, Santiago JG. Effect of PVP on the electroosmotic mobility of wet-etched glass microchannels. Electrophoresis. 2012;33:3259–62.

SUPPORTING INFORMATION

Additional supporting information can be found online in the Supporting Information section at the end of this article.